Providing charge emission for cloud seeding aircraft

Harrison, R. G. ORCID: https://orcid.org/0000-0003-0693-347X, Alkamali, A. A., Escobar-Ruiz, V. ORCID: https://orcid.org/0000-0003-1336-0921, Nicoll, K. A. ORCID: https://orcid.org/0000-0001-5580-6325 and Ambaum, M. H. P. ORCID: https://orcid.org/0000-0002-6824-8083 (2024)
Providing charge emission for cloud seeding aircraft. AIP Advances, 14 (9). 095307. ISSN 2158-3226 doi: 10.1063/5.0227533 Available at https://centaur.reading.ac.uk/117796/

RESEARCH ARTICLE | SEPTEMBER 11 2024

Providing charge emission for cloud seeding aircraft

R. Giles Harrison ; Ahmad A. Alkamali; Veronica Escobar-Ruiz ; Keri A. Nicoll ; Maarten H. P. Ambaum

AIP Advances 14, 095307 (2024)
https://doi.org/10.1063/5.0227533

Providing charge emission for cloud seeding aircraft

Cite as: AIP Advances 14, 095307 (2024); doi: 10.1063/5.0227533
Submitted: 9 July 2024 • Accepted: 14 August 2024 •
Published Online: 11 September 2024

R. Giles Harrison,[1,a)] Ahmad A. Alkamali,[1,2] Veronica Escobar-Ruiz,[1] Keri A. Nicoll,[1] and Maarten H. P. Ambaum[1]

AFFILIATIONS

[1] Department of Meteorology, University of Reading, Whiteknights RG6 6ET, United Kingdom
[2] Department of Research and Weather Enhancement, National Center of Meteorology, Abu Dhabi, UAE

[a)] **Author to whom correspondence should be addressed:** r.g.harrison@reading.ac.uk

ABSTRACT

Releasing charge into natural droplet systems such as fog and clouds offers a route to influence their properties. To facilitate charge release across a wide range of altitudes and meteorological circumstances—such as developing clouds—a charge emitter has been developed for integration with the conventional cloud-seeding flares carried by crewed cloud-seeding aircraft. This allows charge emitters to be used alongside, or instead of, conventional particle releasing flares. The charge emitter flare system is self-contained and self-powered, and includes internal monitoring and recording of its operating parameters. Using this "flare emitter" approach, successful charge emission has been demonstrated in level flight, at 3 km altitude, likely to have exceeded natural ion concentrations by several orders of magnitude. This quantitative verification of successful charge emission can underpin further physically based experiments on the effectiveness of charge release in cloud seeding.

I. INTRODUCTION

In water-stressed regions, cloud seeding is sometimes used to encourage or enhance rainfall.[1] Conventional seeding materials include salt or silver iodide, released from an aircraft with an underwing burning flare, ignited in flight. Our recent work demonstrates that modifying or generating the electric charge on water drops in clouds provides a possible alternative methodology, as charge can encourage droplet coalescence, expediting raindrop growth.[2] Droplet size spectra may be influenced more generally,[3,4] as charge on droplets reduces their evaporation rates, and, through Rayleigh explosions,[5] may even lead to droplet disintegration.

Air in the lower atmosphere contains positive and negative cluster ions at concentrations of about 100 to 1000 cm^{-3} [6] at the surface, generated by radioactivity and cosmic rays. At flight altitudes of 3–5 km, where the loss of ions by aerosol collection is less than that at the surface but at which height cosmic ray ionization has not begun to significantly increase,[7] the ion concentrations become 1500–2000 cm^{-3}.[8] Some charging of atmospheric aerosols and any water droplets present will result from attachment of the ions, in a system that resembles weak dusty plasma. By introducing further ions artificially, a new route to influence the behavior of natural droplet systems becomes possible. The charge release can be achieved through corona emission at atmospheric pressure, using a high voltage source with suitable emitter electrodes, deployed either at the surface[9] or aloft.[10] Release at altitude allows the critical regions of developing clouds to be targeted.

Testing the effectiveness of these approaches requires a suitable airborne platform to provide access to developing clouds. A first step is to establish reliable and controlled charge emission at altitude from such a platform. The use of a crewed aircraft is evaluated here, using a Beechcraft King Air C90 seeding aircraft, operated by the National Center for Meteorology (NCM) in the United Arab Emirates (UAE). Cloud seeding aircraft such as this are typically modified to carry a set of flares in racks below their wings, Fig. 1(a). The conventional flares release material after a brief (timescale ~1 min) period of combustion, electrically ignited by the pilot from the aircraft's cockpit. No meteorological information is recorded by these aircraft.

In this paper, devices with a physical form compatible with the conventional flare mounting rack are demonstrated to provide a straightforward method for charge emission in flight. Section II

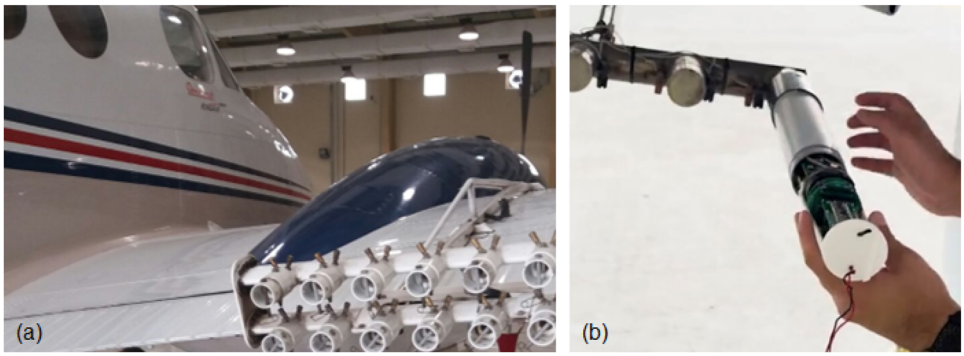

FIG. 1. (a) Beechcraft King Air C90 aircraft modified for cloud seeding missions, showing a flare rack under the wing that carries up to 24 conventional seeding flares. (b) Installation of a flare emitter in the lowered flare rack.

outlines the concept of the devices, and Sec. III summarizes their deployment in a series of test flights. Section IV provides case study data from a clear air test flight. The results and applications are discussed further in Secs. V and VI.

II. FLARE EMITTER

The existing mounting tubes for the conventional cloud-seeding flares provide a volume that can be repurposed for a charge emission device, removing the need for further structural change to the cloud-seeding aircraft. A charge releasing flare—or "flare emitter"—has been developed[11] to occupy the same space, and physically compatible with the fixings used for conventional flares [Fig. 1(b)]. Each flare tube position includes a single electrical connection to the pilot's cockpit controls. This is used to ignite the conventional flare by supplying a short pulse of current to heat a fine wire within the flare. This same connection and initiation pulse are used to trigger the flare emitter.

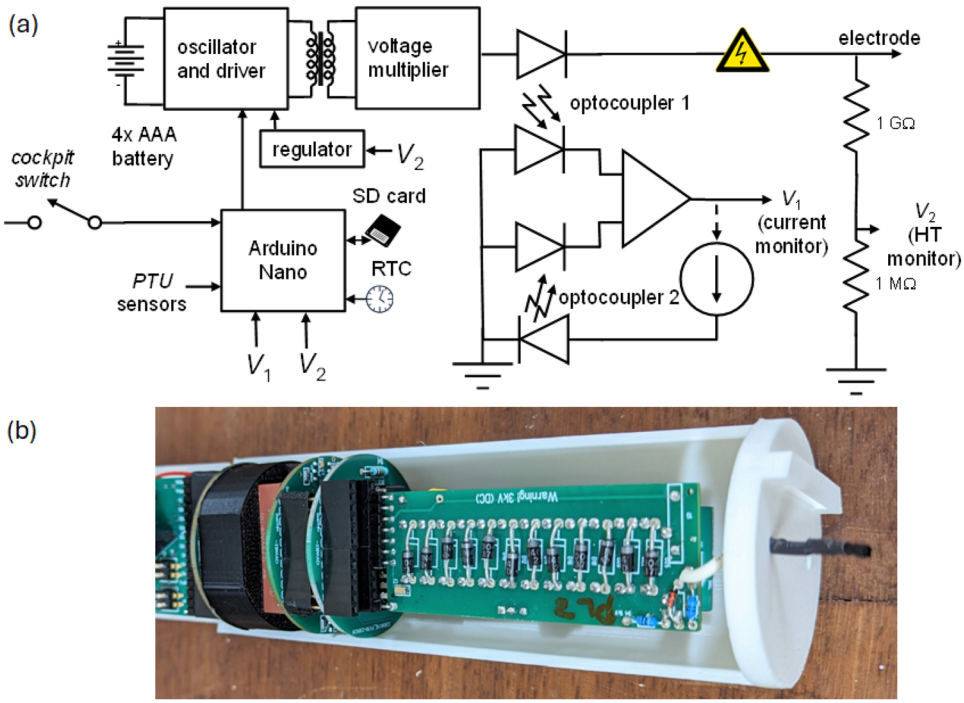

FIG. 2. (a) Block diagram of the flare emitter system. This is activated by a switch that triggers microcode in an Arduino Nano microcontroller module. The Nano also samples pressure, temperature, relative humidity (PTU) sensors, the emitter current (at V_1), and high tension (HT) emitter voltage from a 1000:1 divider (V_2). (V_2 is also used to adjust the driver oscillator to provide regulation of the HT.) Data obtained are written to a microSD card, time-stamped from a real time clock (RTC). (b) Principal aspects of the charge flare emitter, generating the HT voltage for the brush electrode (right). The transformer is to the left of the image, with the Arduino Nano further to the left, just out of shot. (No output current measuring circuitry is implemented in the version shown.) The printed housing fits in the standard 270 mm × 55 mm flare tube.

As the flare emitter is expected to be deployed by individuals whose primary skillset is associated with conventional flares, they are designed to be stand-alone devices, able to be operated without training. To provide data with which they can be subsequently evaluated, the flare emitters contain their own basic meteorological sensors and data logging to record operating parameters and conditions.

The flare emitter operates by corona emission, delivering a regulated high voltage (~3 kV) to a carbon brush electrode, which is found empirically to be sufficient in the laboratory at the surface. As the breakdown electric field for air decreases with pressure,[12] the voltage required will be reduced. This high voltage, selectable for either polarity, is generated from internal batteries using a compact 6 V mains transformer in reverse and twelve stages of Cockroft–Walton voltage multipliers (Fig. 2). Electronic component choices in the design phase were restricted to standard parts due to pandemic-related supply problems.

Figure 2(a) provides a block diagram of the systems within the flare emitter. An Arduino Nano is programmed to control the system and record and timestamp internal pressure, temperature, and relative humidity ("PTU") measurements, with the battery voltage, emitter voltage, and electrode current. The data values obtained are written to an internal microSD card for subsequent analysis. Emission current monitoring is achieved by using an infra-red LED as a current sensor. This provides optical isolation and, through an analog feedback method, compensation for non-linearities and temperature variations.[13] Figure 2(b) shows the physical arrangement.

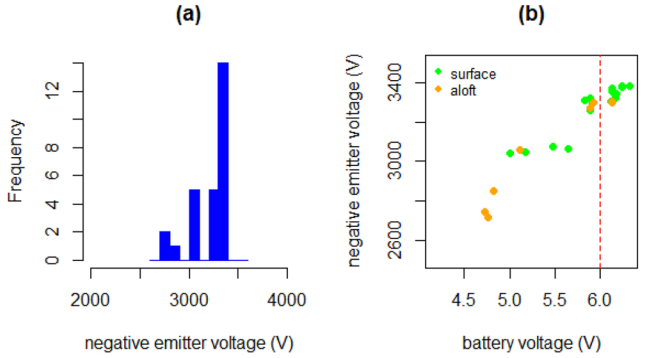

FIG. 3. Distribution of voltages obtained at the negative emitter for (a) all test activations (27 in total) and (b) plotted against battery voltage for values obtained in flight at operating altitude (orange points) and at the surface (green points). Each sample is a median value during the 60 s emitter operating time.

III. EMITTER FLARE DEPLOYMENT

Flights carrying the flare emitters on a King Air aircraft were undertaken in August and September 2023, from Al Ain airport in the UAE (24.25°N, 55.61°E). Positive and negative flare emitters were mounted in the flare tubes that were nearest to the aircraft fuselage, alongside conventional flares, and grounded to the aircraft chassis. To operate the flare emitter, a trigger pulse from the cockpit

TABLE I. Comparison of negative emitter operating voltages at the surface and aloft.

Circumstances[a]	Number of activations	Number of different days	Median pressure (hPa)	Median internal temperature (°C)	Median internal RH (%)	Median emitter voltage (V) for battery voltage >6 V
Aloft	8	2	685	24.5	26	3301
Surface	19	7	978	26.0	30	3353

[a]The distinction between values at the surface and aloft was made from the internal measurement of pressure P, with the flare emitter system considered to be at the surface for $P > 900$ hPa and aloft for $P < 900$ hPa.

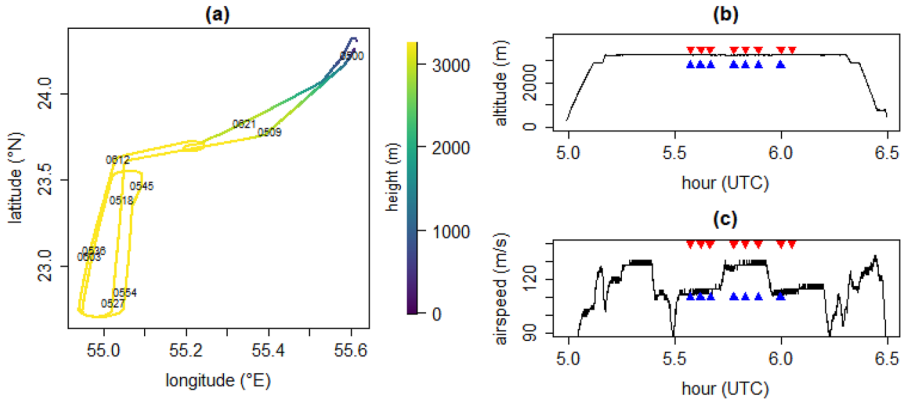

FIG. 4. (a) Trajectory of aircraft leaving Al Ain on September 16, 2023 at 05 UTC, flying south-west before undertaking a period of level flight. (b) Flight altitude and (c) airspeed. Red and blue arrows mark the times when the positive and negative charge emitters, respectively, were triggered by the pilot (quantities derived from aircraft positioning system).

selector switch initiated the microcontroller. As this pulse was generated in the cockpit with a direct connection to the aircraft systems, the signal was optically isolated at the flare emitter for safety and to reduce noise carried back to the cockpit. After the trigger pulse was received, the flare emitter operated for 120 s, with the high voltage activated for the first 60 s only. During the 120 s of operation, data from the sensors and internal monitoring were recorded on the microSD card at a 10 Hz sampling rate.

During the campaign, the flare emitters were operated on the runway and in flight. Runway activations were made on six different days (on 14, 28, and 31 Aug and 3, 4, and 5 Sept) and in-flight activations on two flights (28 Aug and 16 Sept). Emitter voltages recorded from the negative emitter on these occasions are summarized in Fig. 3: the positive flare emitter voltage was unfortunately insufficient to generate reliable corona and was not considered further. Figure 3(a) shows that, despite the regulation system implemented in the circuitry, the negative emitter voltage varied. This is investigated further in Fig. 3(b). Emitter voltages are plotted against the battery voltage, separately for those obtained in flight and those obtained at the surface.

An effect of declining battery voltage on emitter voltage is apparent in both sets of data. If, as is evident from Fig. 3(b), the emitter voltage data are restricted to those when the battery voltage was 6 V or greater, the emitter voltages are similar in both the aloft and surface cases (see also Table I). Regulation of the emitter voltage therefore becomes less effective as the battery ages. This is because the regulation works by temporarily deactivating the oscillator stage whenever the emitter voltage is above a prescribed operating value, which reduces power consumption and enhances reliability by reducing voltage stress on components.[14] If this operating value is not reached due to a weak battery, the regulation ceases and the emitter voltage will decline as the battery voltage declines. This indicates a need for additional multiplier stages in a revised design.

IV. FLIGHT DEPLOYMENT

The detailed operation of the flare emitter during a flight was investigated during the flight on 16th September. This day was chosen for clear air conditions to remove complicating effects due to cloud. The surface relative humidity at 06 UTC was <45% and decreased with height (see also Fig. S1).

The flight departed from Al Ain at about 05 UTC and traveled southwest to a holding position over the southeast of the UAE, where several loops of level flight at 3 km altitude were made [Fig. 4(a)]. The flare emitters were operated intermittently during this period of level flight [Fig. 4(b)], with some variation in air speed [Fig. 4(c)]. Flare emitter operations during the flight were identified from samples of the internal Real Time Clock in the data file generated. The aircraft returned to Al Ain, landing at 0630 UTC.

Each operation of the flare emitter during the flight lasted 60 s, with data recorded for a further 60 s after which the system went back into standby mode. Figure 5 summarizes the data obtained during the seven in-flight runs of the flare emitter on 16th Sep, 2023. Figure 5(a) shows that the battery supply was initially above 6 V, and decreased by almost 1 V through the series of activations. Figure 5(b) shows that the electrode voltage was initially steady but that it decreases proportionally with the declining battery voltage. Figure 5(c) shows that a median emitter current of >3 μA was sustained, also declining with the deterioration in the battery voltage.

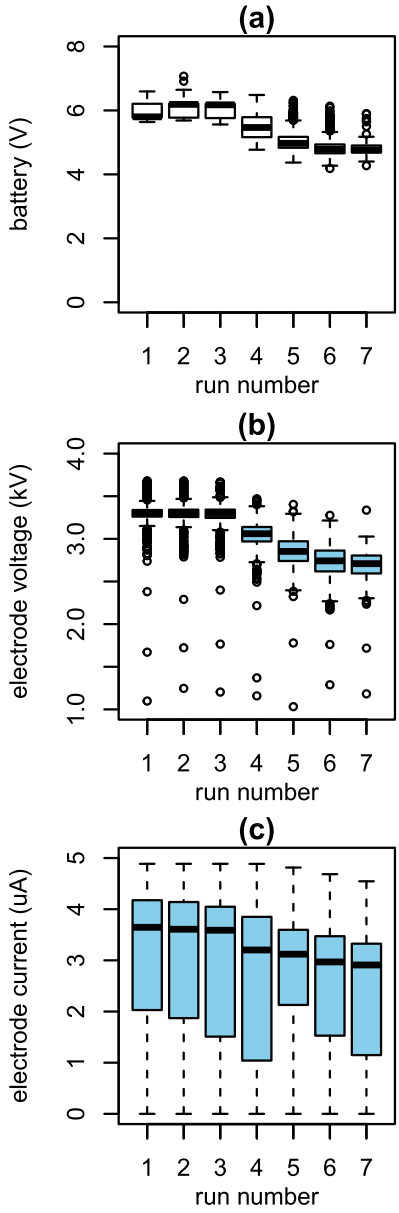

FIG. 5. Boxplots of (a) battery voltage, (b) emitter voltage, and (c) emitter current for the negative ionizer activations during the flight shown in Fig. 3. Thick lines show medians, and the boxes represent the inter-quartile range. Whiskers indicate the outliers.

More details of the flare emitter operation for the full 120 s of run 5 is provided in Fig. 6. Figure 6(a) shows the rapid onset and switch-off of the high voltage on the electrode during the first 60 s. It is clear that there is variability in the high voltage during the operating time. There is a decline in the mean voltage of about 9%, which is

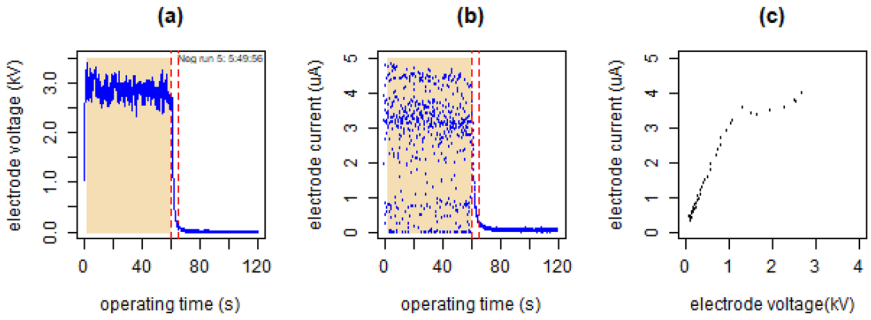

FIG. 6. Time series during 120 s operating burst 5 (on-time shaded) in flight of the negative flare emitter, showing (a) emitter voltage and (b) emitter current. In (c), the voltage–current relation is shown from the end of the emitter operation by plotting those data values at 60–65 s [between the red dashed lines in (a) and (b)] against each other.

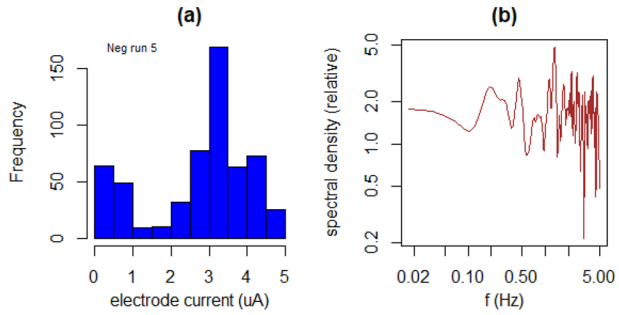

FIG. 7. (a) Histogram of emitter currents from the operating phase identified in Fig. 6(b). (b) Smoothed periodogram of the time series data.

likely to be associated with the regulation matters mentioned earlier due to the driver oscillator operating continuously and draining the battery. Figure 6(b) shows the measured electrode current during the same interval. As for the electrode voltage, there is variability, with a central tendency of ~3 μA, as also evident from the median value for run 5 given in Fig. 5(c). Figure 6(c) extracts the voltage–current relationship, from the decay in emitter voltage at the end of the operating time. Although these data points will have been smoothed by the measurement system, this shows the transition for 1 kV or more on the electrode, to an emission current plateau at ~3 μA.

In Fig. 7(a), histogram of the emitter currents from run 5 is given, which emphasizes that a modal value is well defined. Figure 7(b) provides a spectrum derived from the same data, showing that the variability is essentially white across the range of frequencies available with 10 Hz sampling.

V. DISCUSSION

Monitoring of the emitter voltage in flight demonstrates that the emitter current is highly variable. This is associated with the corona discharge process and ion emission, rather than the measuring system, as it is absent when the high voltage is switched off. Although there is variability in the high voltage supply, variability is a fundamental expectation of corona discharge in general,[15,16] and it is also known to be affected by air speed,[17] which in this case is substantial (~100 ms^{-1}).

Despite the observed variability, a central tendency of emitter current from Figs. 5(c) and 6(b) is apparent and ~3 μA. Assuming emission occurred into 1 m^2, the charge released by a single flare at 120 ms^{-1} would be $1.5 \times 10^{11} e\ m^{-3}$. This can be compared with atmospheric ion concentrations at the flight level of ~10^9 m^{-3}.[8] Hence, the artificial introduction of ions is likely to lead to ion concentrations about two orders of magnitude greater than the natural background.

VI. CONCLUSION

This series of experiments demonstrates that the flare emitter concept provides a device that can release charge under pilot control during a flight and that is straightforwardly fitted to an existing cloud seeding aircraft. Furthermore, the devices provide a quantitative indication of the charge emitted. By deploying a set of multiple flare emitters on a single aircraft, ion concentrations that are considerably enhanced over the natural background can be readily delivered into developing clouds in a controlled way.

SUPPLEMENTARY MATERIAL

Co-located meteorological data for the case study flight is provided as an atmospheric profile in the supplementary material.

ACKNOWLEDGMENTS

This material is based on work supported by the National Center of Meteorology, Abu Dhabi, UAE, under the UAE Research Program for Rain Enhancement Science (UAEREP). The highlight image obtained in flight and Fig. 1(b) were provided by NCM.

AUTHOR DECLARATIONS

Conflict of Interest

The authors have no conflicts to disclose.

Author Contributions

R. Giles Harrison: Conceptualization (equal); Investigation (equal); Methodology (equal); Supervision (equal); Writing – original draft (equal); Writing – review & editing (equal). **Ahmad A. Alkamali**: Data curation (equal); Investigation (equal); Resources (equal); Writing – review & editing (equal). **Veronica Escobar-Ruiz**: Data curation (equal); Resources (equal); Software (equal); Writing – review & editing (equal). **Keri A. Nicoll**: Conceptualization (equal); Funding acquisition (equal); Methodology (equal); Supervision (equal); Writing – review & editing (equal). **Maarten H. P. Ambaum**: Funding acquisition (equal); Project administration (equal); Supervision (equal); Writing – review & editing (equal).

DATA AVAILABILITY

Data is available from the University of Reading data archive,[18] at https://doi.org/10.17864/1947.001337. The co-located meteorological data was obtained from Copernicus Climate Change Service (C3S), as ERA5 hourly data on single levels from 1940 to present. Climate Data Store (CDS), DOI: 10.24381/cds.adbb2d47 (Accessed 20th Feb 2024).

REFERENCES

[1]Y. Wehbe, S. Griffiths, A. Al Mazrouei, O. Al Yazeedi, and A. Al Mandous, "Rethinking water security in a warming climate: Rainfall enhancement as an innovative augmentation technique," npj Clim. Atmos. Sci. **6**(1), 171 (2023).

[2]M. H. P. Ambaum, T. Auerswald, R. Eaves, and R. G. Harrison, "Enhanced attraction between drops carrying fluctuating charge distributions," Proc. R. Soc. A **478**(2257), 20210714 (2022).

[3]P. Wang, C. Li, J. Li, M. Zhang, Y. Yang, and K. Yu, "Electrostatic effects of corona discharge on the spectrum and density evolution of water droplets in air," IEEE Access **8**, 196264 (2020).

[4]R. G. Harrison, G. J. Marlton, M. H. P. Ambaum, and K. A. Nicoll, "Modifying natural droplet systems by charge injection," Phys. Rev. Res. **4**, L022050 (2022).

[5]D. Duft, T. Achtzehn, R. Müller, B. A. Huber, and T. Leisner, "Coulomb fission: Rayleigh jets from levitated microdroplets," Nature **421**(6919), 128 (2003).

[6]U. Hõrrak, J. Salm, and H. Tammet, "Statistical characterization of air ion mobility spectra at Tahkuse observatory: Classification of air ions," J. Geophys. Res.: Atmos. **105**(D7), 9291, https://doi.org/10.1029/1999jd901197 (2000).

[7]G. A. Bazilevskaya, I. G. Usoskin, E. O. Flückiger, R. G. Harrison, L. Desorgher, R. Bütikofer, M. B. Krainev, V. S. Makhmutov, Y. I. Stozhkov, A. K. Svirzhevskaya, N. S. Svirzhevsky, and G. A. Kovaltsov, "Cosmic ray induced ion production in the atmosphere," Space Sci. Rev. **137**(1–4), 149 (2008).

[8]J. M. Rosen, D. J. Hofmann, and W. Gringel, "Measurements of ion mobility to 30 km," J. Geophys. Res. **90**(D4), 5876, https://doi.org/10.1029/jd090id04p05876 (1985).

[9]R. Chambers, S. Beare, S. Peak, and M. Al-Kalbani, "Using ground-based ionisation to enhance rainfall in the Hajar Mountains, Oman," Arabian J. Geosci. **9**(7), 491 (2016).

[10]R. G. Harrison, K. A. Nicoll, G. J. Marlton, D. J. Tilley, and P. Iravani, "Ionic charge emission into fog from a remotely piloted aircraft," Geophys. Res. Lett. **49**(19), e2022GL099827, https://doi.org/10.1029/2022gl099827 (2022).

[11]K. A. Nicoll, V. Escobar-Ruiz, R. G. Harrison, M. H. Ambaum, and A. A. Alkamali, "A charge emitter for use in evaluating aircraft rainfall enhancement," J. Phys. Conf. Ser. **2702**(1), 012005 (2024).

[12]F. Paschen, "Ueber die zum Funkenübergang in Luft, Wasserstoff und Kohlensäure bei verschiedenen Drucken erforderliche Potentialdifferenz," Ann. Phys. **273**(5), 69–96 (1889).

[13]R. G. Harrison, V. Escobar-Ruiz, K. A. Nicoll, and M. H. P. Ambaum, "Isolated corona current monitoring using a compensated light-emitting diode as an unpowered sensor," Rev. Sci. Instrum. **94**(9), 094504 (2023).

[14]R. G. Harrison, "Meteorological radiosonde interface for atmospheric ion production rate measurements," Rev. Sci. Instrum. **76**(12), 126111 (2005).

[15]N. G. C. Ferreira, P. G. C. Almeida, M. S. Benilov, V. A. Panarin, V. S. Skakun, V. F. Tarasenko, and G. V. Naidis, "Computational and experimental study of time-averaged characteristics of positive and negative DC corona discharges in point-plane gaps in atmospheric air," IEEE Trans. Plasma Sci. **48**(12), 4080 (2020).

[16]A. O. Kokovin, A. V. Kozyrev, V. Y. Kozhevnikov, and N. S. Semeniuk, "Characteristics of stationary negative corona discharge in atmospheric air," in *Proceedings of 8th International Congress on Energy Fluxes And Radiation Effects (EFRE–2022)* (Tomsk Polytechnic University, 2022), pp. 550–553, https://doi.org/10.56761/EFRE2022.S5-P-019502.

[17]C. Guerra-Garcia, N. C. Nguyen, T. Mouratidis, and M. Martinez-Sanchez, "Corona discharge in wind for electrically isolated electrodes," J. Geophys. Res.: Atmos. **125**(16), e2020JD032908, https://doi.org/10.1029/2020jd032908 (2020).

[18]R. G. Harrison, A. A. Alkamali, V. Escobar-Ruiz, K. A. Nicoll, and M. H. P. Ambaum (2024). "Charge emission data from 2023 Al Ain Campaign," University of Reading Research Data Archive. https://doi.org/10.17864/1947.001337.